Pharm Res (2010) 27:2466–2477
DOI 10.1007/s11095-010-0239-y

RESEARCH PAPER

Multicomponent Amorphous Nanofibers Electrospun from Hot Aqueous Solutions of a Poorly Soluble Drug

Deng-Guang Yu • Li-Dong Gao • Kenneth White • Christopher Branford-White • Wei-Yue Lu • Li-Min Zhu

Received: 21 May 2010 / Accepted: 6 August 2010 / Published online: 19 August 2010

ABSTRACT

Purpose To design and fabricate multicomponent amorphous electrospun nanofibers for synergistically improving the dissolution rate and permeation profiles of poorly water-soluble drugs.

Methods Nanofibers were designed to be composed of a poorly water soluble drug, helicid, a hydrophilic polymer polyvinylpyrrolidone as filament-forming matrix, sodium dodecyl sulfate as transmembrane enhancer and mannitol as taste masking agent, and were prepared from hot aqueous co-dissolving solutions of them. An elevated temperature electrospinning process was developed to fabricate the composite nanofibers, which were characterized using FESEM, DSC, XRD, ATR-FTIR, *in vitro* dissolution and permeation tests.

Results The composite nanofibers were homogeneous with smooth surfaces and uniform structure, and the components were combined together in an amorphous state because of the favorable interactions such as hydrogen bonding, electrostatic interaction and hydrophobic interactions among them. *In vitro* dissolution and permeation tests demonstrated that the composite nanofibers had a dissolution rate over 26-fold faster than that of crude helicid particles and a 10-fold higher permeation rate across sublingual mucosa.

Conclusions A new type of amorphous material in the form of nanofibers was prepared from hot aqueous solutions of multiple ingredients using an electrospinning process. The amorphous nanofibers were able to improve the dissolution rate and permeation rate of helicid.

KEY WORDS amorphous nanofibers · dissolution · elevated temperature electrospinning · permeation · poorly soluble drugs

D.-G. Yu (✉) • L.-M. Zhu (✉)
College of Chemistry, Chemical Engineering and Biotechnology
Donghua University
Shanghai 201620, China
e-mail: ydg017@dhu.edu.cn
e-mail: lzhu@dhu.edu.cn

L.-D. Gao
College of Information Science &Technology
Beijing University of Chemical Technology
Beijing 100029, China

K. White • C. Branford-White
Institute for Health Research and Policy
London Metropolitan University
London N7 8DB, UK

W.-Y. Lu
School of Pharmacy Fudan University
Shanghai 201203, China

INTRODUCTION

Poorly water-soluble compounds are difficult to develop as drug products using conventional formulation techniques and are frequently abandoned early in the drug development process (1,2). Numerous advanced functional materials, methodologies, new processes and technologies have been tried in order to provide more effective and versatile ways to handle formulation issues associated with poorly water-soluble molecules (3,4). The application of composite materials and nanotechnology to drug delivery is widely expected to create novel therapeutics capable of changing the landscape for the pharmaceutical and biotechnology industries (5,6). To date, one of the most exciting fields of opportunity where nanomaterials and nanotechnology may enable the development of more effective and safer therapeutics for a myriad of clinical applications is improvement in the dissolution profiles and permeation properties of poorly water-soluble drugs (7).

Nanosizing strategies have been widely used to enhance the dissolution and oral availability of numerous poorly

soluble drugs by enlarging the surface area of the drug powder or changing the crystalline form (7–9). Nanoparticle-based drug delivery systems (DDS) reported in the literature include nanocrystalline particles and nanosuspensions of pure drugs (usually prepared by direct nanosizing of the drug particles), nanoparticles, solid lipid nanoparticles, microemulsions, micelles and nano-encapsulations (often the drugs are distributed in a nano complex and are prepared by co-nanosizing of the drugs with functional pharmaceutical excipients such as polymer, surfactants, phospholipids, etc.) (9–12). Although in the past few years formulating poorly water-soluble compounds using a nanoparticle approach has been attempted, there is a growing need for more effective and versatile ways to handle formulation issues associated with poorly water-soluble molecules (13,14). Composite nanofibers have shown their potential in this field recently (15–18).

Compared to nanoparticle-based DDS, nanofiber-based DDSs have one dimension in the microscopic scale but another dimension in the macroscopic scale. This unique characteristic endows them with both the merits possessed by the DDS at the nanometer scale in altering the biopharmaceutic and pharmacokinetic properties of the drug molecule for favorable clinical outcomes, and also the advantages of conventional solid dosage forms such as easy processing, good drug stability, and ease of packaging and shipping (15). The unpopularity of this type of DDS may be due to the difficulty of fabricating nanofibers using traditional methods, such as drawing, template synthesis, phase separation and self-assembly. The use of electrospinning technology may change this situation in the future.

Electrospinning is not only a simple straight-forward process for fabricating nanofibers, but it also allows the co-processing of polymer mixtures or functional materials and chemical cross-linking, which can provide a variety of pathways for controlling the chemical compositions of the nanofibers and for tailoring nanofiber functions (19–21). The concrete advantages of electrospun nanofiber-based DDS for effective delivery of poorly soluble drugs include 1) very large surface area-to-volume ratio, high porosity with very small pore size, and three-dimensional continuous web structure; 2) a one-step top-down easy manufacturing process; 3) easy adaptation for formulation development for administration using different common routes, i.e. oral, transdermal, transmembrane, injection, and topical applications; 4) with appropriate selection of excipients, co-distribution of different functional pharmaceutical ingredients with the drug molecules in the composite nanofibers, allowing improvement of the poor taste and improvement of both the dissolution profiles and the permeability of poorly soluble drugs; 5) the ability to make the filament-forming matrix from different types of common pharmaceutical polymers; 6) electrospinning as the only method that can be further developed for mass production of continuous nanofibers from various polymers (15–18,21).

On the other hand, although the preparation of electrospun nanofibers and their applications in a wide variety of fields has developed very quickly over the past several years, research has been mainly focused on two aspects. One is to broaden the scope of electrospinning to create nanofibers from a more diverse range of materials, including from a single polymer, from a co-dissolved mixture of two different polymers, and also from small molecules such as phospholipids (19). The second is to create composite nanofibers for a variety of applications, from a polymer matrix imbedded with a particular functional material (detectable marker, inorganic functional materials, drug, etc.) (22). To date, little research has been conducted on the possibility of preparing composite electrospun nanofibers derived from a selection of ingredients, each with its own function or target, which can address a common situation when therapeutic delivery involves a cocktail of active pharmaceutical ingredients.

In this paper, we describe the preparation using an elevated temperature process to electrospin aqueous solutions and characterization of multicomponent amorphous nanofibers. The nanofibers were made from components selected mainly to improve the dissolution rates and the permeation profiles of a poorly soluble drug, helicid.

MATERIALS AND METHODS

Materials

Helicid was obtained from Yunnan Yuxi Wanfang Natural Medicine Co., Ltd.. (production batch No. 070702) (Yunnan, China). Polyvinylpyrrolidone K60 (PVP K60, $\overline{M}_w = 360,000$) and mannitol were purchased from Shanghai Yunhong Pharmaceutical Aids and Technology Co., Ltd. (Shanghai, China). Sodium dodecyl sulfate (SDS) was provided by the Sinopharm Chemical Reagent Co., Ltd. All other chemicals used were analytical grade, and the water was highly purified.

Properties of the Co-dissolving Solutions

The solubility of helicid in pure water, aqueous solutions of 0.5% (w/v) SDS, 9.0% (w/v) PVP, 2.0% (w/v) mannitol, and 0.5% (w/v) SDS+9% (w/v) PVP+2.0% (w/v) mannitol, were measured as a function of temperature.

An excess amount of helicid was added to the solutions. The samples were allowed to shake for 48 hr at different temperatures (20, 40, 60, and 80°C). One ml of the sample solution was drawn and filtered through a 0.22μm

(Millipore, USA) pore size filter and diluted using highly purified water. The drug concentration in the sample was measured at 270 nm by a UV spectrophotometer (Unico Instrument Co. Ltd., Shanghai, China). Standard solutions of helicid in pure water with a concentration of 1, 5, 10, 20, and 30 μg/ml were prepared to set up the calibration curve. Other components, PVP, SDS and mannitol, have no ultraviolet absorbance above 240 nm.

The viscosities, surface tensions and electronic conductivities of a mixture of 5.0% (w/v) helicid, 0.5% (w/v) SDS, 9.0% (w/v) PVP and 2.0% (w/v) mannitol were measured as a function of temperature. The viscosities were measured using a NDJ 279 rotary viscometer (Machinery & Electronic Factory of Tongji University), the surface tensions were determined by a BZY-1 Surface Tension Tensiometer (Shanghai Hengping Instrument & Meter Factory), and the conductivities were assessed using a DDS-11 digital conductivity meter (Shanghai Rex Co-perfect Instrument Co., Ltd.). All the measurements were carried out in triplicate.

Electrospinning Process

Ambient temperature suspensions of helicid in aqueous solutions containing 5.0% (w/v) helicid, 0.5% (w/v) SDS, 9.0% (w/v) PVP and 2.0% (w/v) mannitol were placed in a glass syringe (10 mL) with a metal needle (0.5 mm inner diameter). After heating to 70°C, the solutions were equilibrated for half an hour before starting the electrospinning process (Fig. 1).

A high-voltage power supply (ZGF60KV/2 mA, Shanghai, China) was used at a voltage of 15 kV, and the fibers produced were collected on aluminium foil at a distance of 12 cm. The flow rate was controlled at 2 ml/h by means of a single syringe pump (Cole-Parmer, USA). The resulting non-woven mats were placed in a dessicator.

Casting films for use as controls were prepared by keeping the electrospinning solutions at 70°C for complete drying in an air-circulated oven until reaching a constant weight.

Morphology

The morphology of the surface and the cross-sections of the nanofiber mats and the casting films was assessed using a S-4800 field emission scanning electron microscope (FESEM) (Hitachi, Japan). The average fiber diameter was determined by measuring diameters of composite nanofibers at over 100 points from FESEM images using ImageJ software (National Institutes of Health, USA). Before the carbon-coating process, the cross-sections of the nanofiber mats were prepared by first placing them into liquid nitrogen, and then they were broken manually.

Characterization

The differential scanning calorimetry (DSC) analyses were carried out using an MDSC 2910 differential scanning calorimeter (TA Instruments Co., USA). Sealed samples were heated at 10°C·min^{-1} from 20 to 250°C. The nitrogen gas flow rate was 40 ml·min^{-1}.

X-ray diffraction patterns (XRD) were obtained on a D/Max-BR diffractometer (RigaKu, Japan) with Cu Kα radiation in the 2θ range of 5–60° at 40 mV and 300 mA.

Attenuated total reflectance fourier transform infrared (ATR-FTIR) analysis was carried out on a Nicolet-Nexus 670 FTIR spectrometer (Nicolet Instrument Corporation, Madison, USA) at the scanning range of 500–4,000 cm^{-1} and a resolution of 2 cm^{-1}.

In Vitro Dissolution and Permeation Tests

In vitro dissolution tests were carried out according to the Chinese Pharmacopoeia (2005 ED.) Method II, in which a paddle method using a RCZ-8A dissolution apparatus (Tianjin University Radio Factory, China) was used.

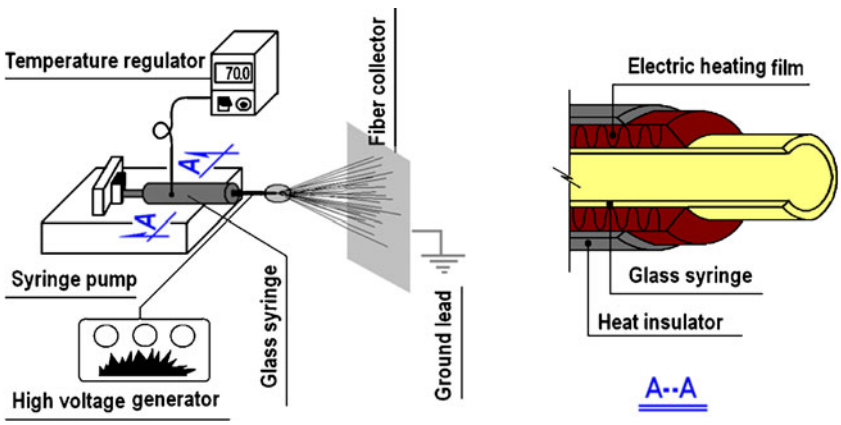

Fig. 1 The elevated temperature electrospinning process.

Three-hundred-and-thirty mg of composite nanofibers or casting films or 100 mg of crude helicid particles (<100 μm) were put into 900 mL phosphate buffer solutions (PBS, pH6.8, 0.1 M) at 37±1°C and at 50 rpm, sink conditions $C<0.2C_s$. At predetermined time points (0, 10, 30, 60, 120, 180, 240, 300, and 360 min), samples of 5.0 ml were withdrawn from the dissolution medium and replaced with fresh medium to maintain constant volume. After filtration through a 0.22 μm membrane (Millipore, USA) and appropriate dilution with PBS, the sample solutions were analyzed at 270 nm by a UV spectrophotometer (Unico Instrument Co. Ltd., Shanghai, China). All the measurements were carried out in triplicate.

The *in-vitro* permeation studies were performed using a RYJ-6A Diffusion Test Apparatus (Shanghai Huanghai Drug Control Instrument Co. Ltd.), in which six Keshary-Chien-type glass diffusion cells were mounted in a water bath system to maintain a constant temperature of 37±0.2°C. Each diffusion cell had a diffusion area of 2.60 cm^2. The receptor compartment had a capacity of 7.2 mL.

Porcine sublingual mucosa obtained from a local slaughterhouse were used within 2 hr of slaughter. The mucosa were mounted between the donor and receptor compartments of the diffusion cell with the mucosal surface uppermost. Each donor compartment was filled with 1 ml PBS. The hydrodynamics in the receptor compartment were maintained by stirring with a Teflon-coated magnetic bead at 100 rpm. The sublingual membranes were equilibrated for 30 min before permeation tests.

Sixteen-mm diameter discs cut from the composite nanofiber membranes or casting films were placed on the mucosal surface. One-ml samples were withdrawn from the receptor compartment at timed intervals, filtered through a 0.22 μm membrane (Millipore, USA) and analyzed at 270 nm by a UV spectrophotometer (Unico Instrument Co. Ltd., Shanghai, China). All the measurements were carried out in triplicate.

RESULTS AND DISCUSSION

For preparing homogeneous composite nanofibers, compatibility among the components is vital. Helicid, the therapeutic ingredient that is the focus of this study, was originally isolated as one of the main active constituents from *Helicid nilgrinica Bedd*, a plant indigenous to western China that has been used for thousands of years for curing headache and insomnia, and no obvious side effects have been reported (23). Helicid is a poorly water-soluble drug. A formulation that allows rapid dissolution and absorption for fast onset of therapeutic action is highly desirable (24).

In the elctrospinning process, PVP acted as the filament-forming matrix and also provided functional groups and sites for "anchoring" little molecules of helicid, SDS and mannitol to form the composite nanofibers and to amorphize them. On the other hand, PVP, SDS and mannitol are all common functional pharmaceutical excipients. SDS is often used as a transmembrane/transdermal enhancer, and mannitol is a sweetener often used for taste masking in oral formulations. The three excipients have good compatibility with each other, and PVP and SDS are often used to improve solubility of poorly soluble drugs (25,26). This suggested that the combined usage of PVP and SDS at an elevated temperature might improve the solubility of helicid synergistically (27,28).

The effects of temperature and the presence of PVP and/or SDS on solubility of helicid are shown in Fig. 2A. While heating alone could increase the solubility of helicid (Fig. 2A curve (a)), the presence of PVP (curve (b)), SDS (curve (c)), or both (curve (d)) enhanced the solubility further. The dominant factor for increasing solubility appears to be temperature. The solubility of helicid (108.7 $g{\cdot}l^{-1}$) in the solution with PVP and SDS at 80°C is over 12-fold higher than the solubility of helicid (8.9 $g{\cdot}l^{-1}$) in water at 20°C. In addition, the presence of mannitol in aqueous solutions has little influence on the solubility of helicid (data not shown).

Solvent selection is often a key factor in determining both the ability of solutions to undergo electrospinning and the structural homogeneity of the nanofibers (17,18). Helicid has poor solubility at ambient temperature, not only in water, but also in common organic solvents such as ethanol, methanol, acetone and chloroform. No common solvents are readily available for making homogeneous solutions suitable at room temperature for electrospinning. On the basis of the data above, and since PVP, SDS and mannitol are all readily soluble in water, hot water was selected as a solvent suitable for co-solution of all components needed for the preparation of fibres.

The second key factor for successful electrospinning is having a sufficient concentration of filament-forming polymers in the solution to ensure adequate interaction between the polymer molecules (18,29). In the present study, PVP K60 was selected as the optimum filament-forming matrix for two reasons. First, compared with PVP K30, it has more C = O groups for H-bonding with helicid and mannitol so that lower concentrations would be needed for electrospinning, thus allowing higher drug-to-polymer ratios in the final composite nanofibers than would be possible with PVP K30. Second, PVP K60 is faster than PVP K90 in leading the helicid molecules to dissolve from the composite nanofibers during the dissolution process, because less time is needed for the polymer molecules with lower molecular weight to absorb water, swell, disentangle, and finally dissolve into the dissolution medium than polymer molecules with a higher molecular weight.

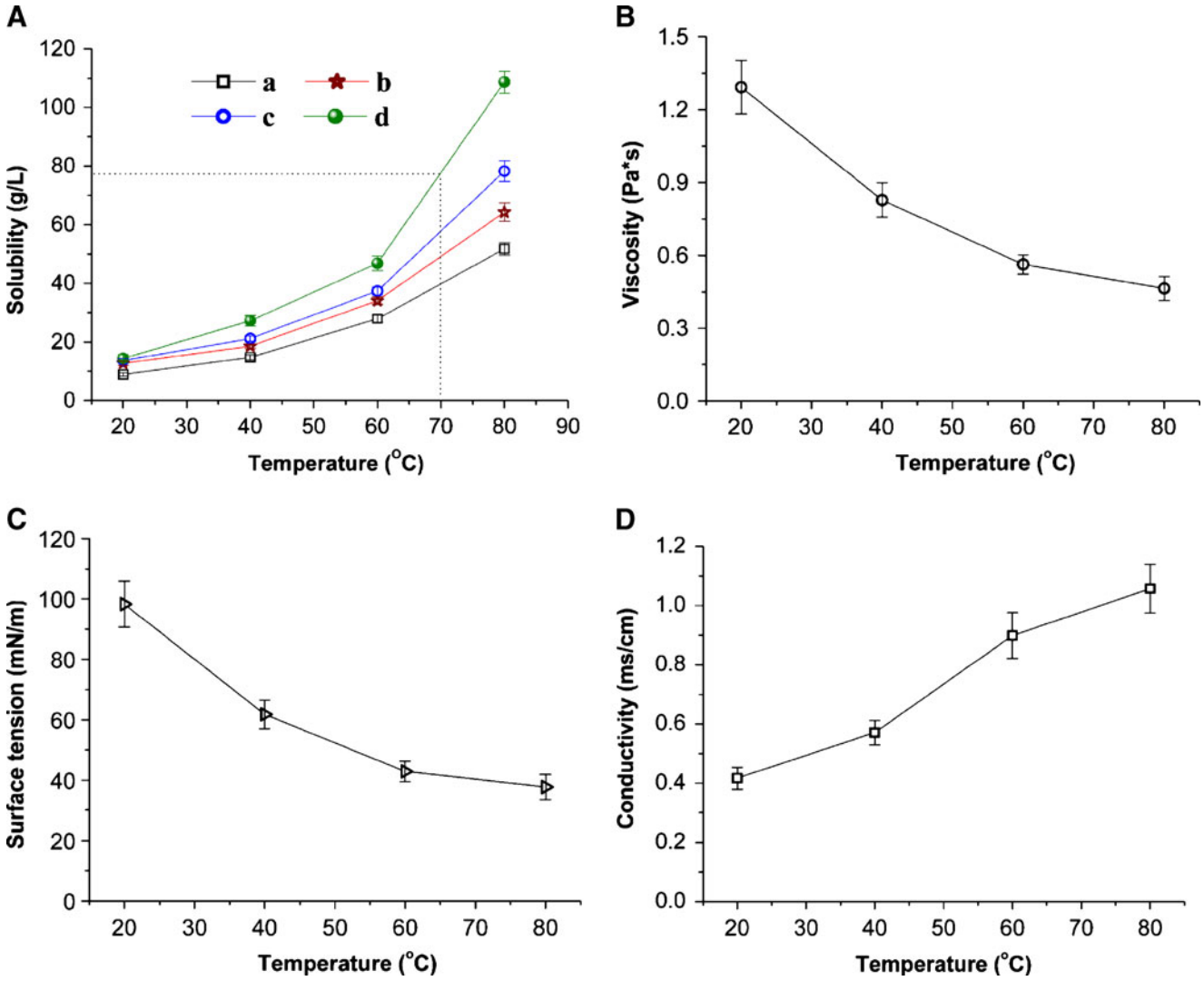

Fig. 2 Properties of multi-ingredient aqueous solutions. (**A**) Temperature dependence of helicid solubility in different aqueous solutions: (a) water only, (b) 0.5% (w/v) SDS, (c) 9.0% (w/v) PVP, (d) 0.5% (w/v) SDS, 9.0% (w/v) PVP and 2.0% (w/v) mannitol. (**B**), (**C**) and (**D**) Effect of temperature on the viscosity, surface tension and conductivity, respectively, of a solution of 5.0% (w/v) helicid, 0.5% (w/v) SDS, 9% (w/v) PVP and 2% (w/v) mannitol ($n = 3$).

Our preliminary experiments using pure PVP solutions at ambient temperature indicated that the lowest concentration for preparing bead-free nanofibers using the electrospinning process for PVP K60 is about 8% (w/v). Moreover, raising the temperature of the solutions had no influence on the chain entanglement status, which is a prerequisite condition for preparing uniform fibers to prevent the capillary breakup (30,31). Nine percent (w/v) PVP K60 solutions were used to ensure that electrospinning of solutions at high temperature was stable. The operating temperature was fixed at 70°C, because (1) temperatures of 80°C or higher are near the boiling point of water and may lead to clogging of the spinning head of the needle capillary tube due to fast evaporation, and (2) according to the results from Fig. 2A(d), the solubility of helicid in the presence of PVP, SDS and mannitol at 70°C was 77.6 $g{\cdot}l^{-1}$, which allows a wide range of helicid concentrations to be accommodated in the DDS. In this study, a helicid concentration of 50 $g{\cdot}l^{-1}$, i.e. 5.0% (w/v) was selected for electrospinning, which is well within the limit of solubility and yet allows a relatively high loading of drug.

As expected, when the temperature increased, the suspensions of helicid gradually dissolved, and the solution viscosities (Fig. 2B) and surface tensions (Fig. 2C) decreased, whereas conductivities (Fig. 2D) increased. All these trends help to improve the electrospinnability of the solutions and to facilitate preparation of composite nanofibers with high quality.

Fig. 3a, b and c show field emission scanning electron microscope (FESEM) images of the composite nanofiber mat surface at different magnifications. The nanofibers have uniform structure without beads-on-a-string morphol-

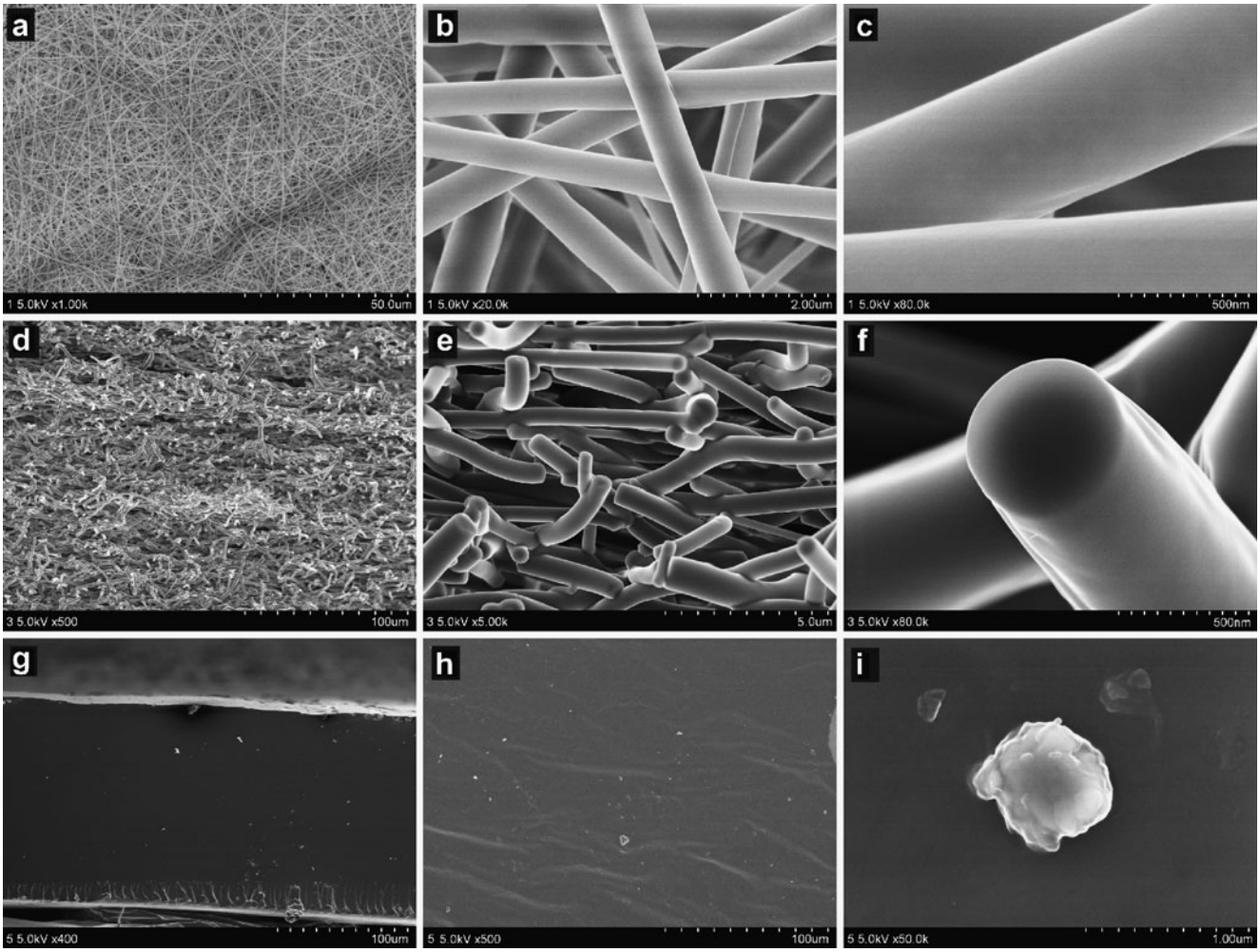

Fig. 3 FESEM images: (**a**), (**b**) and (**c**) surface morphology of composite nanofibers, (**d**), (**e**) and (**f**) cross section of the composite nanofibers, (**g**) cross-section of casting films, (**h**) surface morphology of casting films, (**i**) a typical image of the separated particles in casting films.

ogy and have smooth surfaces without any particles separating out from the nanofiber matrix. About 93% of the nanofibers have a diameter between 400 and 600 nm.

Fig. 3d, e and f, show FESEM images of the cross-section of the composite nanofiber mats at different magnifications. No particles are discernible, indicating that there was no phase separation. This suggests that the functional materials are distributed uniformly through the polymer fiber matrix.

FESEM images of the cross-section (Fig. 3g) and surface morphology (Fig. 3h) of the casting films show particles separated out from the cast films, which could be seen both on the surface and on the cross-section of the casting films. A typical FESEM image of the separated particles found in casting films is shown in Fig. 3i. The particles had an irregular shape and a dimension range from several tens of nanometers to several microns.

The time taken to generate the composite nanofibers by electrospinning from the hot aqueous solution was only several decades of milliseconds. The rapid evaporation of the solvent and the favorable interactions among the ingredients resulted in a solid solution in the form of a three-dimensional continuous web structure of nanofibers, in which helicid, mannitol and SDS molecules are randomly ordered, comparable to the liquid state in the PVP matrix, without any crystal lattice being formed from the solutes.

In contrast, casting films require several hours to reach a constant weight. Moreover, during the casting and evaporation process, it is hard to remove the solvent from the co-precipitates to an acceptable level rapidly because the co-precipitates become more and more viscous during the drying process, which prevents further evaporation of the residual solvent and facilitates local phase separation, resulting in many nanoparticles in the casting films.

To further investigate the physical status of the molecular components, differential scanning calorimetry (DSC) analyses and X-ray diffraction tests (XRD) were conducted.

The DSC thermograms of the individual ingredient, casting films and composite nanofibers are shown in Fig. 4. The DSC curve of pure helicid and mannitol exhibited a single endothermic response corresponding to melting points of 200.11 and 168.58°C respectively. SDS had a melting point of 181.84°C followed closely by a decomposing temperature of 213.24°C. PVP K60 had a broad endotherm due to dehydration, which lies between 80°C and 120°C and with a peak at 86.13°C. PVP is a polymer and can be present in a glassy or rubber state. The change from one state to the other can be detected as a glass transition around 160–180°C depending on its molecular weight (32). This glass transition is not visible in Fig. 4 due to scale and generally is not detected in current DSC. DSC thermograms of both composite nanofibers and casting films did not show any melting peaks of small molecules, but a broad endotherm resulted from the absorbed moisture.

On the other hand, the decomposition bands of SDS in the composite nanofibers and casting films were narrower and higher than that of pure SDS, reflecting that the SDS decomposition rates in nanofibers and casting films are bigger than that of pure SDS. The peak temperatures of decomposition shifted from 213.24°C to 207.58°C for the casting films, and to 205.29°C for the nanofibers, reflecting

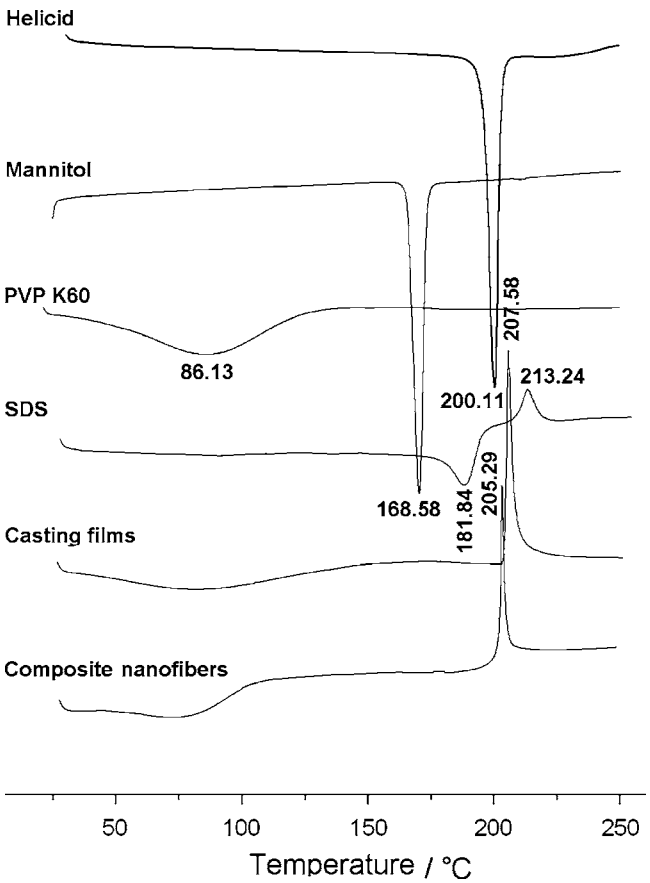

Fig. 4 DSC thermograms.

that the onset of SDS decomposition in nanofibers and casting films is earlier than that of pure SDS. The amorphous state of SDS and highly even distributions of SDS in nanofibers and casting films should make SDS molecules respond to the heat more sensitively than pure SDS particles, and the nanofibers and casting films might have better thermal conductivity than pure SDS. Their combined effects prompted the SDS in nanofibers and casting films to decompose earier and quicker.

Shown in Fig. 5, numerous distinct peaks can be seen in the XRD patterns of helicid, mannitol and SDS because they are crystalline materials. The PVP diffraction exhibits a diffused background pattern with two diffraction halos, which means that the polymer is amorphous (33).

As far as the composite nanofibers and the casting films are concerned, the characteristic peaks of helicid, mannitol and SDS were also completely absent, and only a hump characteristic of amorphous forms was observed. This suggests that all the small molecule components were no longer present as crystalline material, but instead were fully converted into an amorphous state. On the other hand, the shape and the position of the amorphous haloes of the composite nanofibers and the casting films are different from the pure PVP. The amorphous halo at 11.26° was completely absent in the XRD patterns of the composite nanofibers and the casting films, reflecting the change of the orientation, conformation and organization of polymer chains in the amorphous phase, and thus the altering of the amorphous packing density of polymer chains (34).

The results from XRD and DSC suggested that the composite nanofibers were homogeneous and all the small functional molecules (helicid, mannitol and SDS) were distributed through the PVP matrix amorphously, losing their original crystal state as pure materials. The multicomponent composite electrospun nanofibers were totally amorphous materials.

To distinguish the interactions among the different components in the nanofibers and the casting films, attenuated total reflectance fourier transform infrared (ATR-FTIR) analyses were carried out. ATR-FTIR spectra of pure materials (PVP, SDS, mannitol and helicid), the composite nanofibers and the casting films are shown in Fig. 6. The presence of hydrogen bonding interactions in the composite nanofibers between PVP and helicid, PVP and mannitol, SDS and helicid, and SDS and mannitol can be inferred from the disappearance of peaks within the 3,000–4,000 cm^{-1} regions assigned to the O-H stretching vibrations in mannitol and helicid, as well as from the shifts to lower wavenumbers of peaks assigned to the C = O stretching vibrations at 1,657 cm^{-1} from 1,668 cm^{-1} of helicid and 1,661 cm^{-1} of PVP.

The absorption bands of SDS (C–H stretching) at 2,956, 2,917 and 2,850 cm^{-1} and of PVP (C–H stretching) at 2,953 cm^{-1} disappear in the composite nanofibers com-

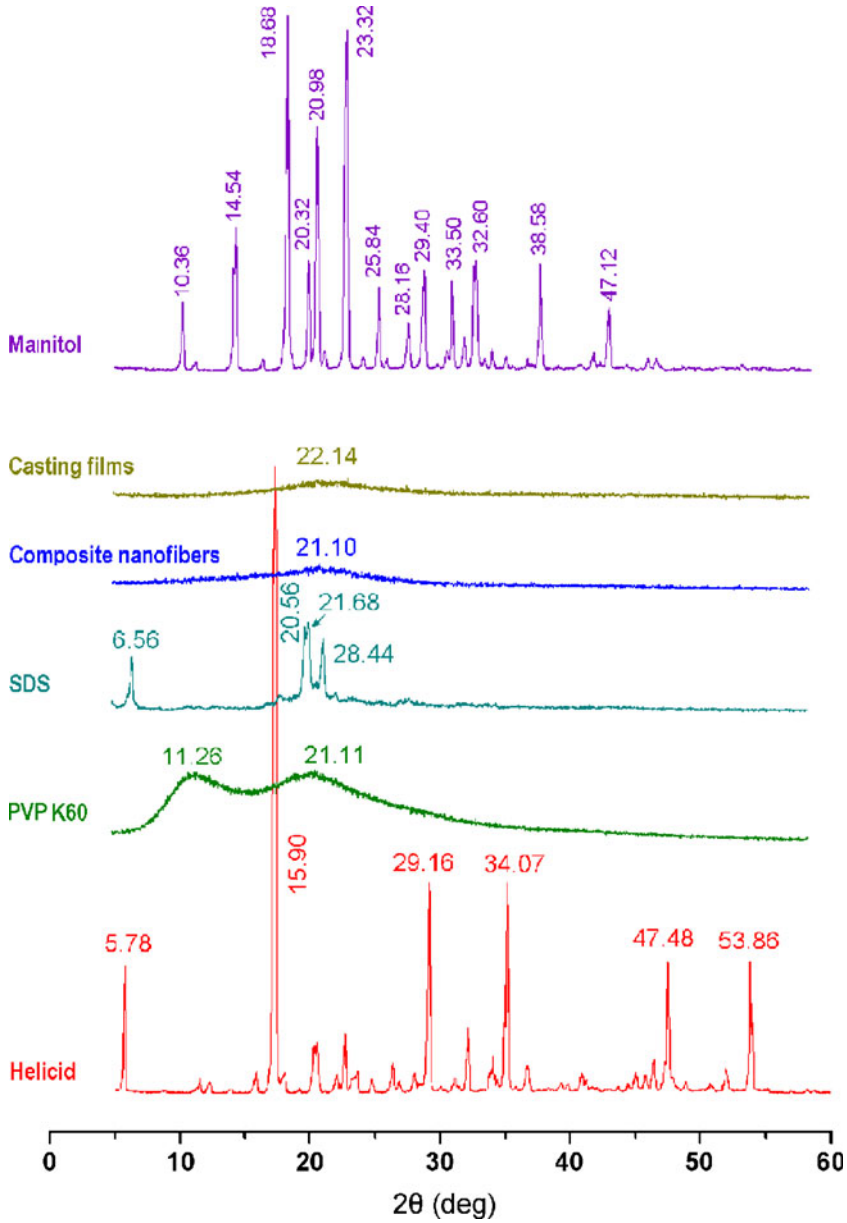

Fig. 5 X-ray diffraction patterns.

pared to the pure SDS and PVP, but a broader and weaker band at 2,924 cm^{-1} appears, indicative of hydrophobic interactions between the PVP and SDS molecules.

The characteristic bands of pure SDS at 1,083 and 1,225 cm^{-1} are due to symmetric (*vs* S–O) and asymmetric (*vs* S–O) stretching of the sulfate group, and are shifted to 1,075 and 1,217 cm^{-1}, respectively, in the composite nanofibers. The changes were attributed to the electrostatic interaction between the negatively charged SDS head group and the nitrogen atom on the pyrrolidone ring of PVP (35), and also the attractive interaction between the negatively charged PVP oxygen (N^+ = C-O^-) and the electron poor C-1′ of SDS (36).

In the spectra of casting films, there are still several small peaks of O-H within 3,000–4,000 cm^{-1}, and the bands at 1,071 and 1,038 cm^{-1} have a stronger intensity than those of the composite nanofibers. The presence in casting films of peaks corresponding to crystalline helicid means that clusters of crystalline helicid (probably as nanocrystals) were still formed in the amorphous structure of the casting films. The molecular mobility and the interactions among the different components in solution are physical and reversible, allowing a thorough mixing of components, whereas the slow evaporation and drying during the process of preparing casting films led to local phase separation, resulting in agglomerations of mixtures of ingredients as observed on the FESEM images and the crystal lattices in the casting films.

Thus, it is the second-order interactions, such as hydrogen bonding, electrostatic interaction and hydrophobic inter-

Fig. 6 ATR-FTIR spectra.

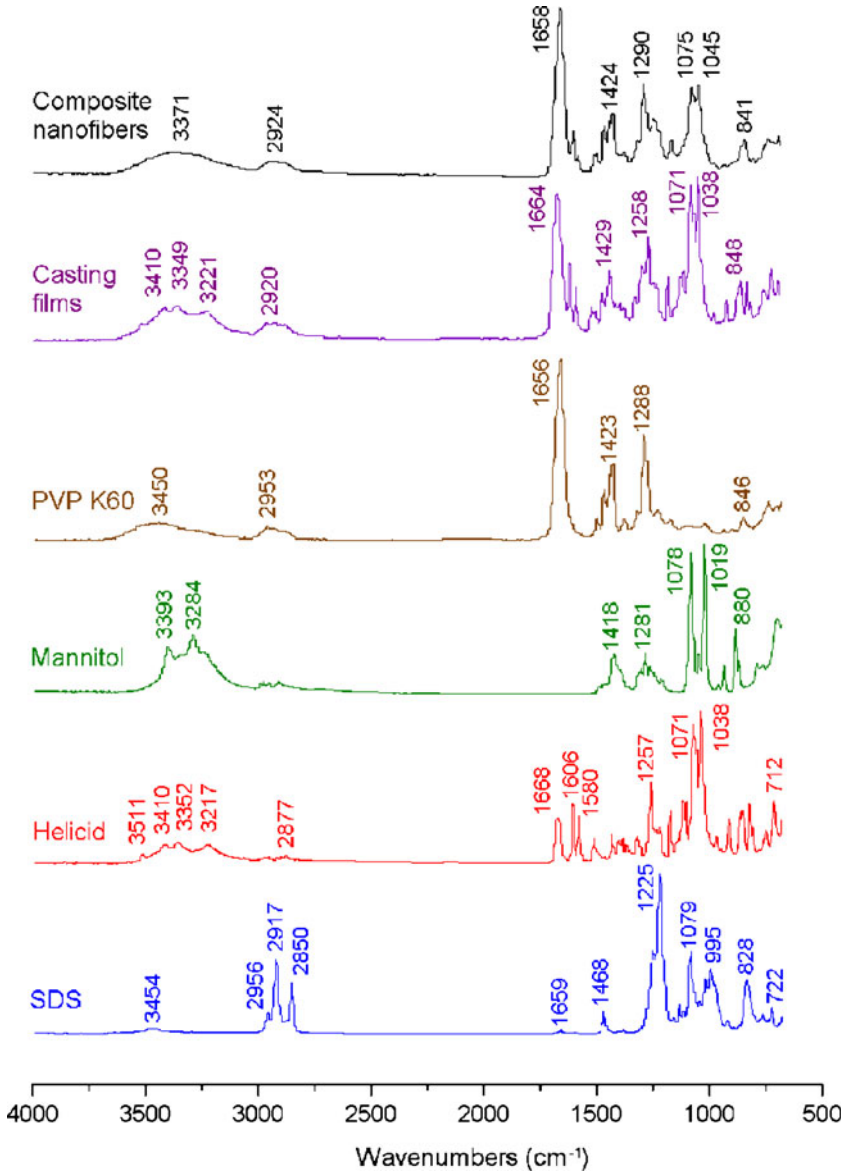

actions, that played a fundamental role in promoting the structural homogeneity of the amorphous nanofibers. In the separated particles of casting films, it is possible that the content of mannitol and helicid was higher than in the bulk of the casting films, which would account for some of the small differences between the ATR-FTIR spectra of casting films and the composite nanofibers.

Fig. 7 shows a comparison of *in vitro* dissolution profiles of helicid from composite nanofibers, casting films, and crude helicid particles (≤100 μm). Dissolution rates of 3.12, 1.55, and 0.12 $mg \cdot min^{-1}$ for the composite nanofibers, casting films, and crude helicid particles, repectively, were calculated from regression of the linear phase of the release time-course.

The dissolution rate of helicid from the composite nanofibers and the casting films was over 26-fold and near 13-fold faster than that from crude particles, respectively. The key factors should be that helicid presented in the nanofibers and the casting films mainly in an amorphous manner, and therefore no crystal lattice energy had to be overcome for dissolution, and that the PVP-SDS-helicid-mannitol complex allowed greatly improved drug wetability. Due to the unique physical characteristics of electrospun nanofiber mats, such as large surface area, high porosity, and steric continuous web structures, which are useful for quickly transferring solvent and drug molecules during the dissolution process, the amorphous nanofibers gave a drug dissolution rate twice as fast as the casting films. Methods for improving drug solubility or dissolution rate continue to be highly sought after (37,38); electrospun amorphous nanofibers can provide a useful strategy for this purpose, and here the especial merit is that the preparation process was free of organic solvents.

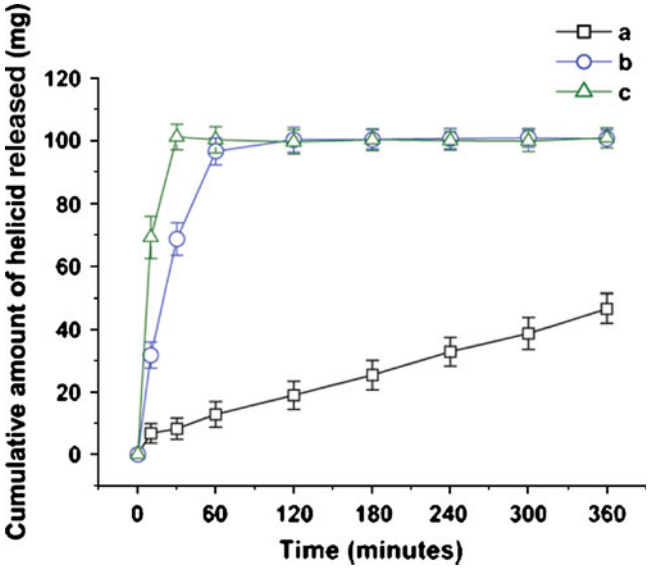

Fig. 7 *In vitro* dissolution profiles, (**a**) crude helicid particles (≤100 μm); (**b**) casting films; (**c**) composite nanofiber mats ($n=3$).

Sixteen-mm diameter discs were cut from the composite nanofiber mats and the casting films for *in vitro* permeation tests. The casting films had an average thickness of 0.152 ± 0.01 mm and a weight of 32.03 ± 0.34 mg ($n=6$), giving an apparent density of 1.06 mg·cm^{-3}. The electrospun composite nanofibers had a thickness of 0.85 ± 0.04 mm and a weight of 34.41 ± 0.57 mg (continuously electrospinning about 8 h). The apparent densities of the electrospun membrane were 0.201 mg·cm^{-3}. Ten mg of the pure helicid particles were spread on the mucosal surface evenly as control.

Fig. 8 shows a comparison of *in vitro* permeation profiles across porcine sublingual mucosa of helicid released from composite nanofibers, casting films, and crude helicid particles. The cumulative percentages of helicid transferred across the membrane after the first hour were 50.3%, 18.4% and 5.8% for the composite nanofibers, casting films, and crude helicid particles, respectively. Regressed from the linear time periods of transfer, the permeation equations for the composite nanofibers, casting films, and crude helicid particles were $Q=0.08448t-0.0204$ ($R=0.9978$, $t\leq 60$ min), $Q=0.02767t+0.01715$ ($R=0.9880$, $t\leq 180$ min), $Q=0.00803t+0.06588$ ($R=0.9992$, $t\leq 360$ min), respectively, where Q is the proportion of helicid transferred, and t is the time in min. Thus, the composite nanofibers, casting films, and crude helicid particles had a linear permeation rate of 32.5, 10.6, and 0.3 μg·min^{-1}·cm^{-2}, respectively.

The apparent permeability coefficient (P) could be calculated using the following equation (39,40):

$$P = \frac{dQ/dt}{C_0 A}$$

where dQ/dt is the steady-state flux, C_0 is the initial donor concentration, and A is the diffusion area. The apparent permeability coefficient for composite nanofibers, casting films and the helicid particles were 5.41×10^{-5}, 1.76×10^{-5} and 5.17×10^{-6} cm·s^{-1}, respectively, indicating that the composite nanofibers yielded a permeation rate of helicid that was over 10-fold faster than that of the crude particles and three-fold faster than the casting films. The faster permeation rates from the composite nanofibers than form the casting films can be explained by the fact that permeability across the sublingual mucosa is a passive diffusion process, and hence faster dissolution of helicid would lead to an increased concentration gradient of drug at the mucosal surface, which would facilitate rapid partitioning of drug into the sublingual mucosa and subsequent permeation (41). The SDS released from the nanofibers may also improve permeation by extracting intercellular lipids that act as a rate-limiting barrier to the transport of helicid molecules (42).

CONCLUSIONS

This study has demonstrated that it is possible to combine helicid, PVP, SDS, and mannitol to create uniform, composite nanofibers from their hot aqueous solutions using an electrospinning process. The synergistic effects of raised temperature and the presence of PVP and SDS in the solutions not only improved the solubility of helicid, but also facilitated the electrospinning process through favourable changes in the viscosity, surface tensions and conductivity of the solutions. The composite nanofibers had a uniform structure with no beads-on-a-string morphology and no

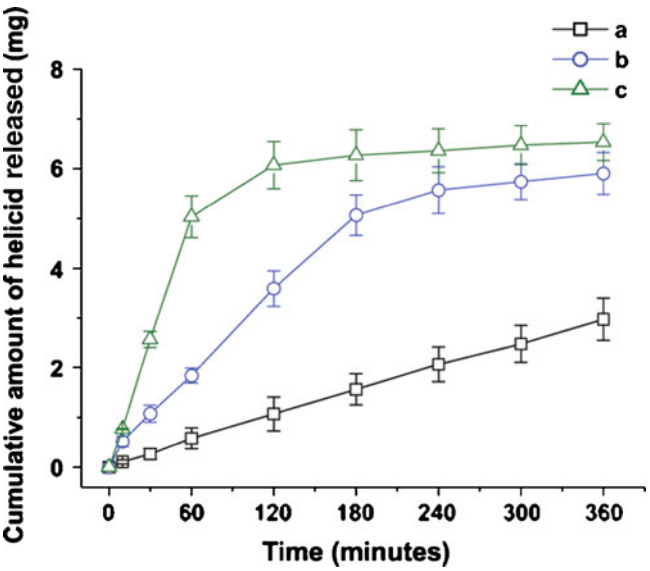

Fig. 8 *In vitro* permeation profiles: (**a**) crude helicid particles (≤100 μm); (**b**) casting films; (**c**) composite nanofibers ($n=3$).

particles arising from phase separation. XRD and DSC results demonstrated that helicid, SDS and mannitol were mixed together in the composite nanofibers in an amorphous manner. The ATR-FTIR spectra verified that second-order interactions, such as hydrogen bonding, electrostatic interaction and hydrophobic interactions, occurred among the components and likely play a significant role in promoting the structural homogeneity of the nanofibers. The amorphous state of the nanofibers and the PVP-SDS-helicid-mannitol composites allowing improved drug wetability made their *in vitro* drug dissolution rate and permeation rate be over 26-fold and 10-fold higher than that of crude helicid particles, respectively. The unique physical characteristics of nanofibers, such as large surface area, high porosity and assembling in a three-dimensional continous web structure, made their *in vitro* drug dissolution rate and permeation rate be 2-fold and 3-fold higher than that of casting films, respectively. The report here provides an example of the systematic design, preparation, characterization and application of a novel type of amorphous materials, which has the potential to provide a useful strategy for enhancing the absorbance of poorly water-soluble drugs and to be further developed to prepare novel DDS.

ACKNOWLEDGEMENTS

This work was financially supported by China Postdoctoral Science Foundation Project (Special NO. 200902195) and UK-CHINA Joint Laboratory for Therapeutic Textiles.

REFERENCES

1. Tang B, Cheng G, Gu JC, Xu CH. Development of solid self-emulsifying drug delivery systems: preparation techniques and dosage forms. Drug Discov Today. 2008;13:606–12.
2. Rasenack N, Muller BW. Dissolution rate enhancement by *in situ* micronization of poorly water-soluble drugs. Pharm Res. 2002;19:1894–900.
3. Vasconcelos T, Sarmento B, Costa P. Solid dispersions as strategy to improve oral bioavailability of poor water soluble drugs. Drug Discov Today. 2007;12:1068–75.
4. Blagden N, de Matas M, Gavan PT, York P. Crystal engineering of active pharmaceutical ingredients to improve solubility and dissolution rates. Adv Drug Del Rev. 2007;59:617–30.
5. Merisko-Liversidge E, Liversidge GG, Cooper ER. Nanosizing: a formulation approach for poorly-water-soluble compounds. Eur J Pharm Sci. 2003;18:113–20.
6. Farokhzad OC. Nanotechnology for drug delivery: the perfect partnership. Expert Opin Drug Del. 2008;5:927–9.
7. Farokhzad OC, Langer R. Impact of Nanotechnology on Drug Delivery. ACS Nano. 2009;3:16–20.
8. Moshfeghi AA, Peyman GA. Micro- and nanoparticulates. Adv Drug Deliv Rev. 2005;57:2047–52.
9. Merisko-Liversidge E, McGurk SL, Liversidge GG. Insulin nanoparticles: a novel formulation approach for poorly water soluble Zn-insulin. Pharm Res. 2004;21:1545–53.
10. Yin L, Ding J, He C, Cui L, Tang C, Yin C. Drug permeability and mucoadhesion properties of thiolated trimethyl chitosan nanoparticles in oral insulin delivery. Biomaterials. 2009;30:5691–700.
11. Li H, Zhao X, Ma Y, Zhai G, Li L, Lou H. Enhancement of gastrointestinal absorption of quercetin by solid lipid nanoparticles. J Control Release. 2009;133:238–44.
12. Li P, Hynes SR, Haefele TF, Pudipeddi M, Royce AE, Serajuddin AT. Development of clinical dosage forms for a poorly water-soluble drug II: formulation and characterization of a novel solid microemulsion preconcentrate system for oral delivery of a poorly water-soluble drug. J Pharm Sci. 2009;98:1750–64.
13. Merisko-Liversidge E, Liversidge GG. Drug nanoparticles: formulating poorly water-soluble compounds. Toxicol Pathol. 2008;36:43–8.
14. Amidon GL, Lennernäs H, Shah VP, Crison JR. A theoretical basis for a biopharmaceutic drug classification: the correlation of *in vitro* drug product dissolution and *in vivo* bioavailability. Pharm Res. 1995;12:413–20.
15. Yu DG, Shen XX, Branford-White C, White K, Zhu LM, Bligh SWA. Oral fast-dissolving drug delivery membranes prepared from electrospun polyvinylpyrrolidone ultrafine fibers. Nanotechnology. 2009;20:055104.
16. Yu DG, Branford-White C, White K, Li XL, Zhu LM. Comparison of solid dispersions in drug delivery membranes from different processes. AAPS PharmSciTech. 2010;11:809–17.
17. Yu DG, Branford-White C, Li L, Wu XM, Zhu LM. The compatibility of acyclovir with the matrix polymer PAN in the electrospun nanofiber membrane. J Applied Polym Sci. 2010;117:1509–15.
18. Yu DG, Zhu LM, White K, Branford-White C. Electrospun nanofiber-based drug delivery systems. Health. 2009;1:67–75.
19. McKee MG, Layman JM, Cashion MP, Timothy EL. Phospholipid nonwoven electrospun membranes. Science. 2006;311:353–5.
20. Dzenis Y. Spinning continuous fibres for nanotechnology. Science. 2004;304:1917–9.
21. Rutledge GC, Fridrikh SV. Formation of fibers by electrospinning. Adv Drug Del Rev. 2007;59:1384–91.
22. Ji L, Saquing C, Khan SA, Zhang X. Preparation and characterization of silica nanoparticulate–polyacrylonitrile composite and porous nanofibers. Nanotechnology. 2008;19:085605.
23. Liu DY, Wang GL, Ma SC, Lin RC. Research on the pharmaceutical active components in Helicia Lour. Chin Tradit Herbal Drugs. 2004;35:593–5.
24. Yu DG, Yang XL, Wang Y, Li X, Xu HB. 3DP used for controlled-release helicid tablets. Chin Tradit Patent Med. 2007;29:679–83.
25. Chawla G, Bansal AK. Improved dissolution of a poorly water soluble drug in solid dispersions with polymeric and non-polymeric hydrophilic additives. Acta Pharm. 2008;58:257–74.
26. Whitehea K, Karr N, Mitragotri S. Safe and effective permeation enhancers for oral drug delivery. Pharm Res. 2008;25:1782–8.
27. Pongpeerapat A, Wanawongthai C, Tozuka Y, Moribe K, Ymamoto K. Formation mechanism of colloidal nanoparticles obtained from probucol/PVP/SDS ternary ground mixture. Int J Pharm. 2008;352:309–16.
28. Wanawongthai C, Pongpeerapat A, Higashi K, Tozuka Y, Moribea K, Yamamoto K. Nanoparticle formation from probucol/PVP/sodium alkyl sulfate co-ground mixture. Int J Pharm. 2009;376:169–75.
29. Li D, Xia Y. Electrospinning of nanofibers: reinventing the wheel? Adv Mater. 2004;16:1151–70.
30. Wang C, Chien HS, Hsu CH, Wang YC, Wang CT, Lu HA. Electrospinning of polyacrylonitrile solutions at elevated temperatures. Macromolecules. 2007;40:7973–83.

31. Givens SR, Gardner KH, Rabolt JF, Chase DB. High-temperature electrospinning of polyethylene microfibers from solution. Macromolecules. 2007;40:608–10.
32. Jadhav NR, Gaikwad VL, Nair KJ, Kadam HM. Glass transition temperature: basics and application in pharmaceutical sector. Asian J Pharm. 2009;3:82–9.
33. McKee MG, Elkins CL, Long TE. Influence of self-complementary hydrogen bonding on solution rheology/electrospinning relationships. Polymer. 2004;45:8705–15.
34. Murthy NS, Minor H, Bednarczyk C, Krimm S. Structure of the amorphous phase in oriented polymers. Macromolecules. 1993;26:1712–21.
35. Pongpeerapat A, Higashi K, Tozuka Y, Moribe K, Yamamoto K. Molecular interaction among probucol/PVP/SDS multicomponent system investigated by solid-state NMR. Pharm Res. 2006;23:2566–74.
36. Roscigno P, Asaro F, Pellizer G, Ortana O, Paduano L. Complex Formation between PVP and sodium decyl sulfate. Langmiur. 2003;19:9638–44.
37. Verreck G, Chun I, Peeters J, Rosenblatt J, Brewster ME. Preparation and characterization of nanofibers containing amorphous drug dispersion generated by electrostatic spinning. Pharm Res. 2003;20:810–7.
38. Ghebremeskel AN, Vemavarapu C, Lodaya M. Use of surfactants as plasticizers in preparing solid dispersions of poorly soluble API: selection of polymer–surfactant combinations using solubility parameters and testing the processability. Int J Pharm. 2007;328:119–29.
39. Goswami T, Jasti BR, Li X. Estimation of the theoretical pore sizes of the porcine oral mucosa for permeation of hydrophilic permeants. Arch Oral Biol. 2009;54:577–82.
40. Dhiman MK, Dhiman A, Sawant KK. Transbuccal delivery of 5-fluorouracil: permeation enhancement and pharmacokinetic study. AAPS PharmSciTech. 2009;10:258–65.
41. Chett DJ, Chen LH, Chien YW. Characterization of captopril sublingual permeation of preferred routes and mechanisms. J Pharm Sci. 2001;90:1868–77.
42. Nicolazzo JA, Reed BL, Finnin BC. Buccal penetration enhancers—How do they really work? J Control Release. 2005;105:1–15.